Ultrafast carrier transport in ultrafine porous polymers for highly selective photocatalytic reduction of CO_2 to CH_4

Guoen Tang[a], Huicong Zhang[a], Ting Song[a,*], Shiheng Yin[b], Guojiang Mao[c], Bei Long[a], Atif Ali[d], Guo-Jun Deng[a,*]

a Key Laboratory for Green Organic Synthesis and Application of Hunan Province, Key Laboratory of Environmentally Friendly Chemistry and Application of Ministry of Education, College of Chemistry, Xiangtan University, Xiangtan 411105, P. R. China.

b Analytical and Testing Center, South China University of Technology, Guangzhou 510640, P. R. China.

c School of Chemistry and Chemical Engineering, Henan Normal University, Xinxiang, 453007, P. R. China

d Department of Chemistry and State Key Laboratory of Synthetic Chemistry, The University of Hong Kong, Pokfulam Road, Hong Kong, P. R. China.

*Corresponding author. E-mail: songtg@xtu.edu.cn, gjdeng@xtu.edu.cn

Computational methods

The first-principles calculations based on the Density Functional Theory (DFT) were performed using the Materails Studio software with DMol3 model. The Perdew-Burke-Ernzerhof (PBE) exchange-correlation functional within the generalized gradient approximation (GGA) was employed to describe the exchange-correlation energy. The energy cutoff for the plane wave basis expansion was set to 600 eV. The force on each atom was set as 0.03 eV/Å for convergence criterion. Slab model was constructed in a 4×4 supercell, with a vacuum layer of 20 Å in the z direction to avoid the interaction between layers. The sampling in the Brillouin zone was set with 3×3×1 by the Monkhorst-Pack method. The van der Waals interaction was considered by using DFT-D3 method.

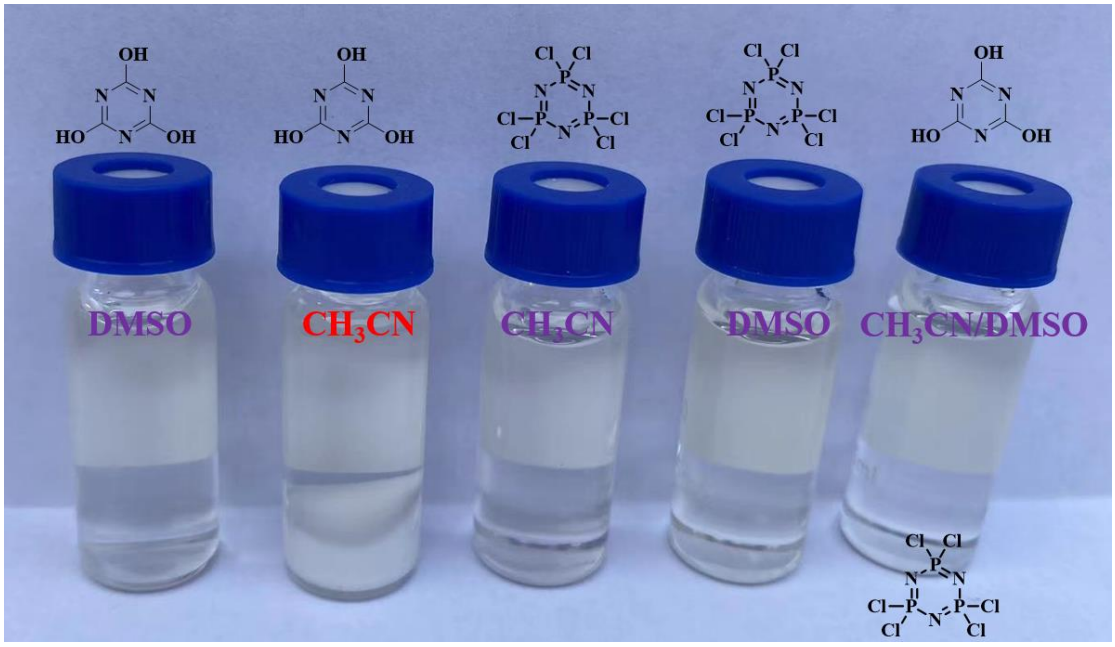

Fig. S1. Picture of the dissolution of cyanuric acid and hexachlorocyclotriphosphazene in a solvent.

Fig. S2. Picture of D1M4-PC sample in the reaction solution.

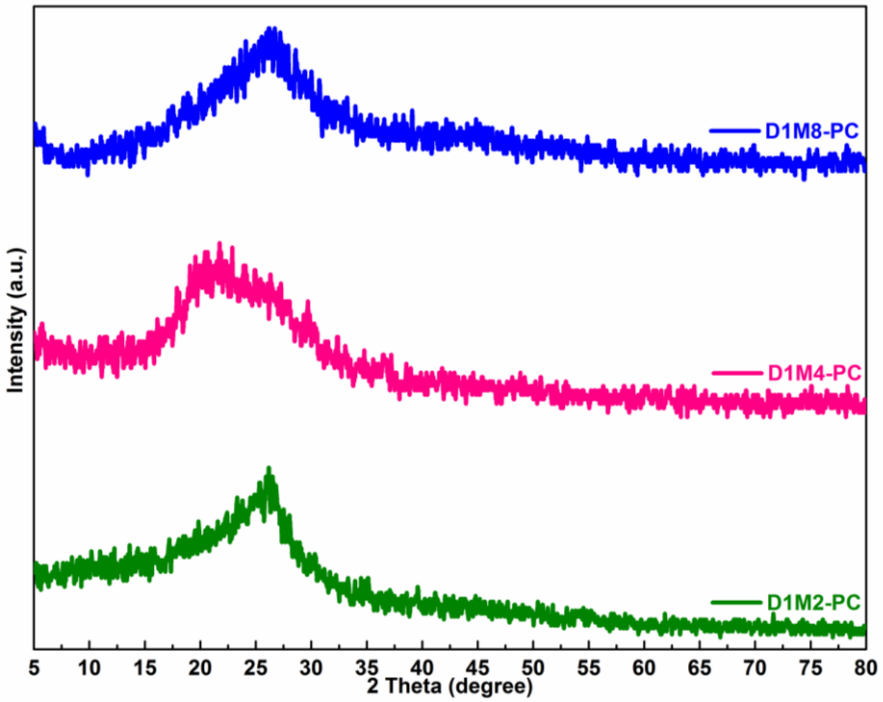

Fig. S3. XRD patterns of D1M2-PC, D1M4-PC and D1M8-PC samples.

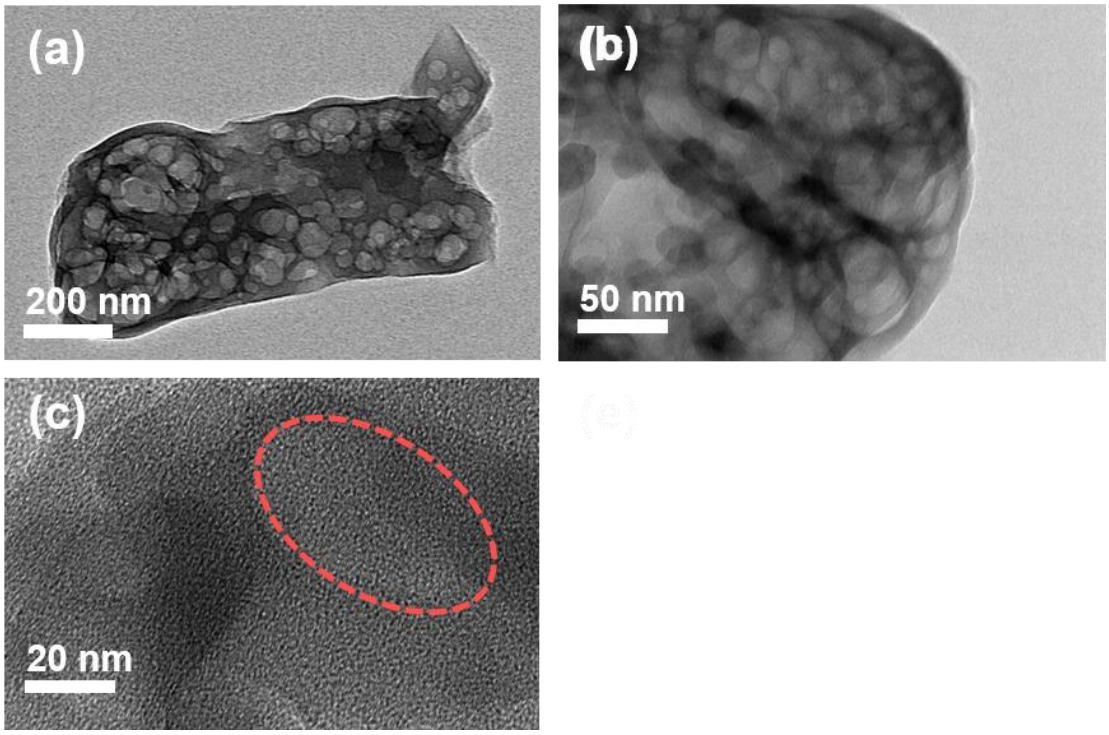

Fig. S4. TEM images (a, b) and HRTEM (c) of D1M2-PC.

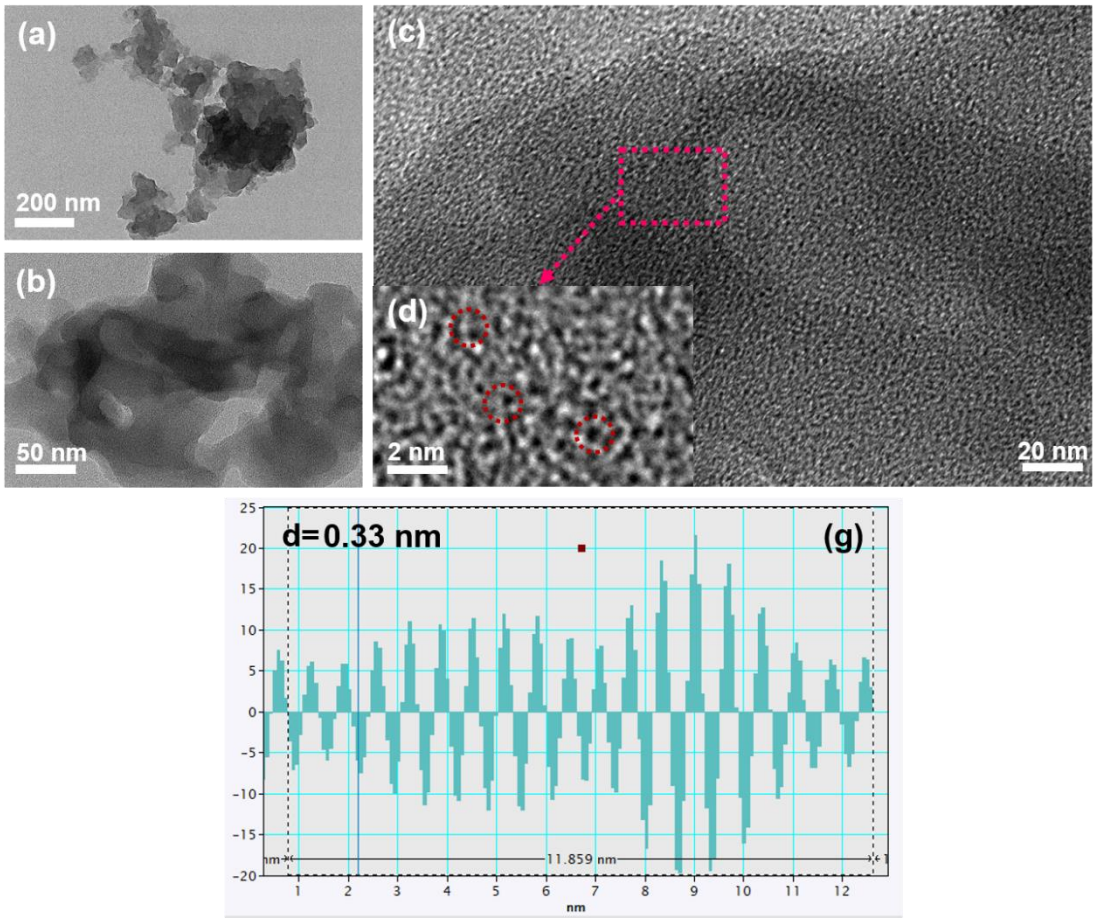

Fig. S5. TEM images (a, b), HRTEM (c and d) and interval length picture (e) of D1M8-PC.

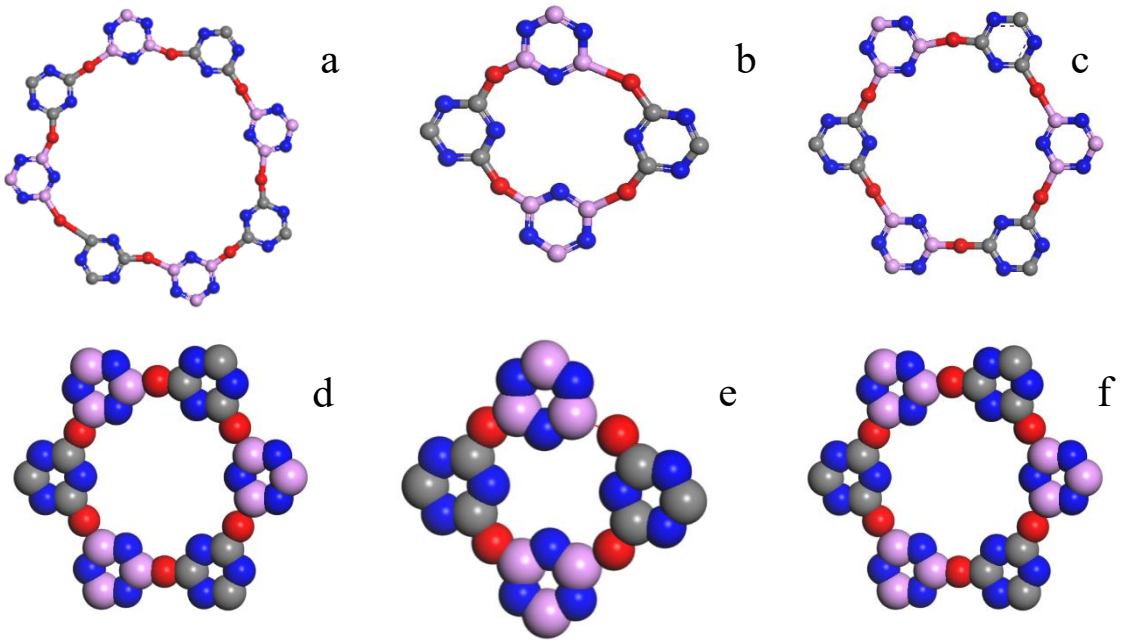

Fig. S6. Ball-stick representation of D1M2-PC, D1M4-PC and D1M8-PC (a-c) and CPK structure of D1M2-PC, D1M4-PC and D1M8-PC (d-f) (N element (Blue), P element (Pink), C element (Gray), and O element (Red)).

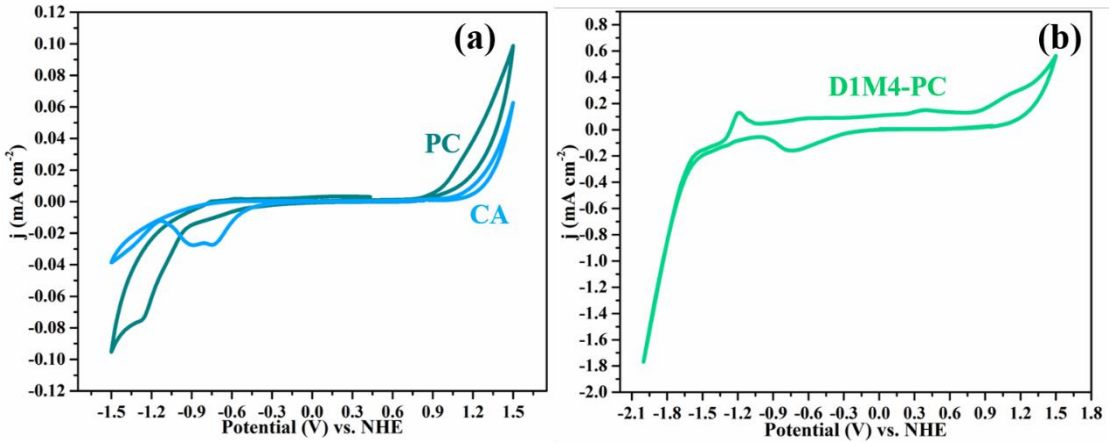

Fig. S7. (a) Cyclic voltammograms (CVs) of cyanuric acid (CA) and hexachlorocyclotriphosphazene (PC) in MeCN solution containing 0.1 M of tetrabutylammonium hexafluorophosphate (TBAHFP). (b) CV of D1M4-PC.

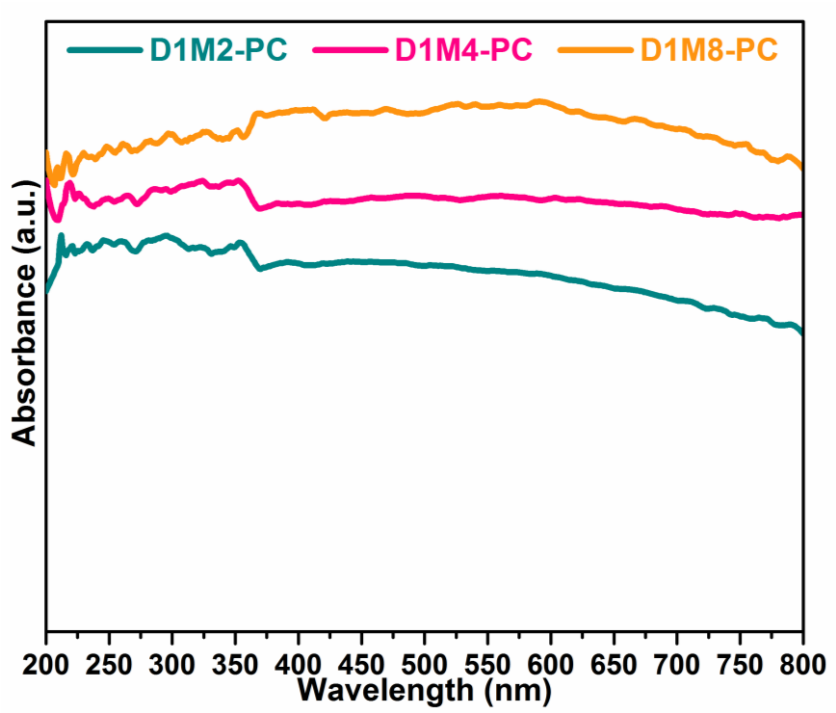

Fig. S8. UV-vis diffuse reflectance spectra (DRS) of D1M2-PC, D1M4-PC and D1M8-PC samples.

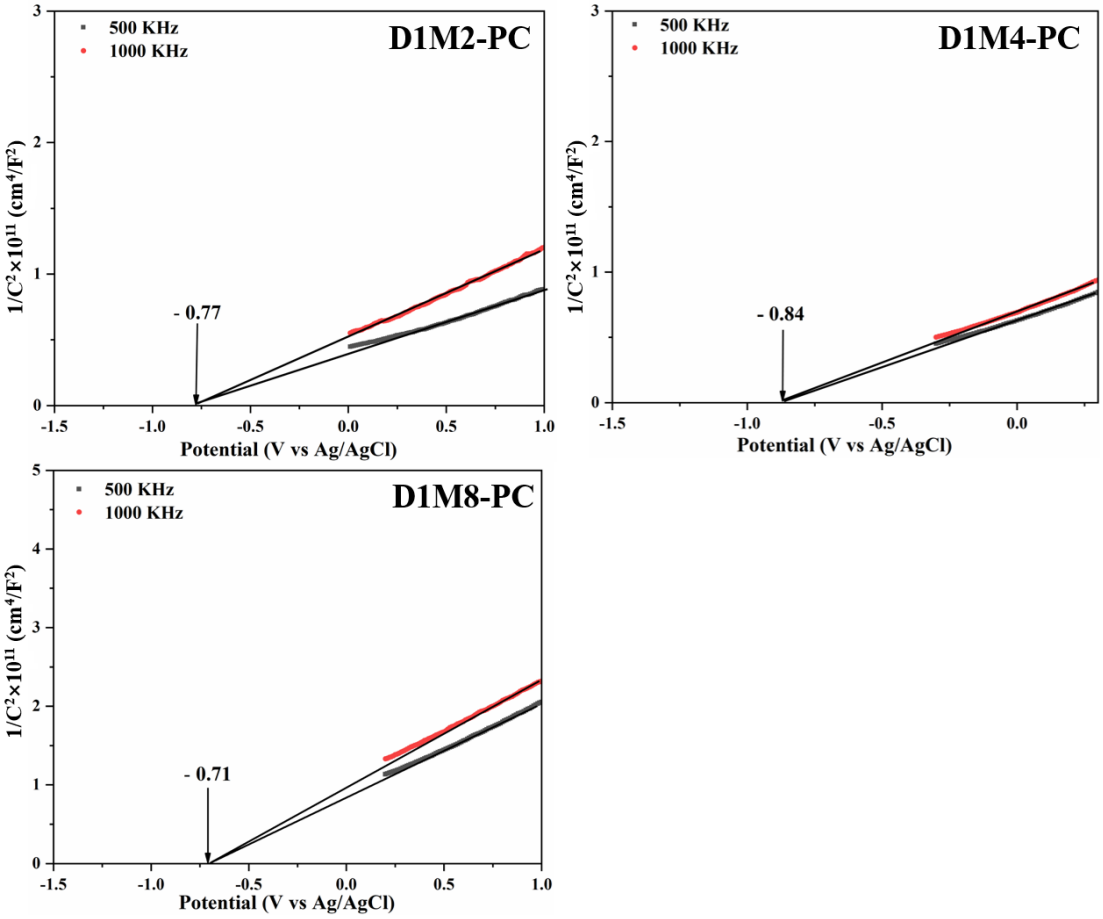

Fig. S9. The Mott-Schottky plots of D1M2-PC, D1M4-PC and D1M8-PC samples.

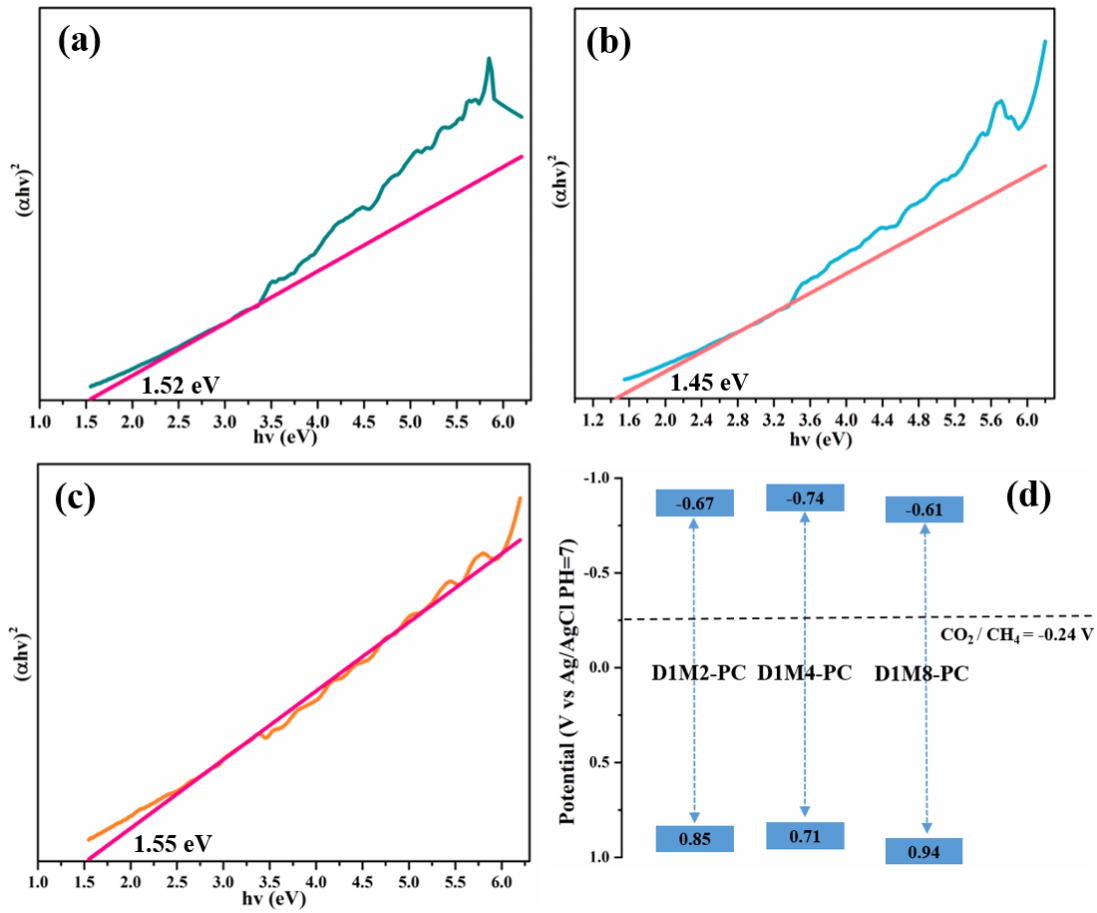

Fig. S10. (a) The $(\alpha h\nu)^2$ versus hv curve of (a) D1M2-PC, (b) D1M4-PC and (c) D1M8-PC samples; The band structure of the compounds is calculated by the KubelKa-Munk (KM) method according to the following equation: $\alpha h\nu = A(h\nu - Eg)^{1/2}$, where α is the absorption coefficient, hv is the photo energy, Eg is the band gap, and A is a constant. (d) The schematic diagram of the calculated band positions of D1M2-PC, D1M4-PC and D1M8-PC samples.

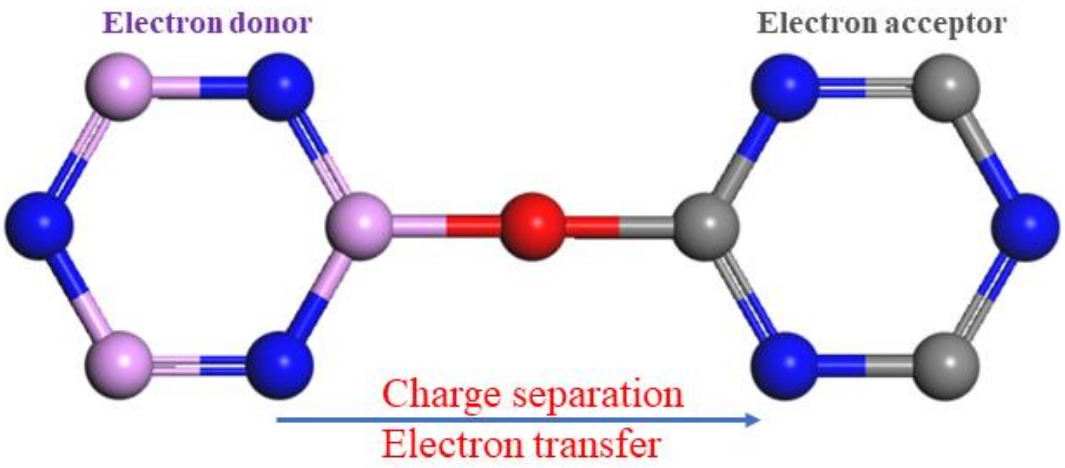

Fig. S11. Donor-acceptor structure of D1M4-PC sample (N element (Blue), P element (Pink), C element (Gray), and O element (Red)).

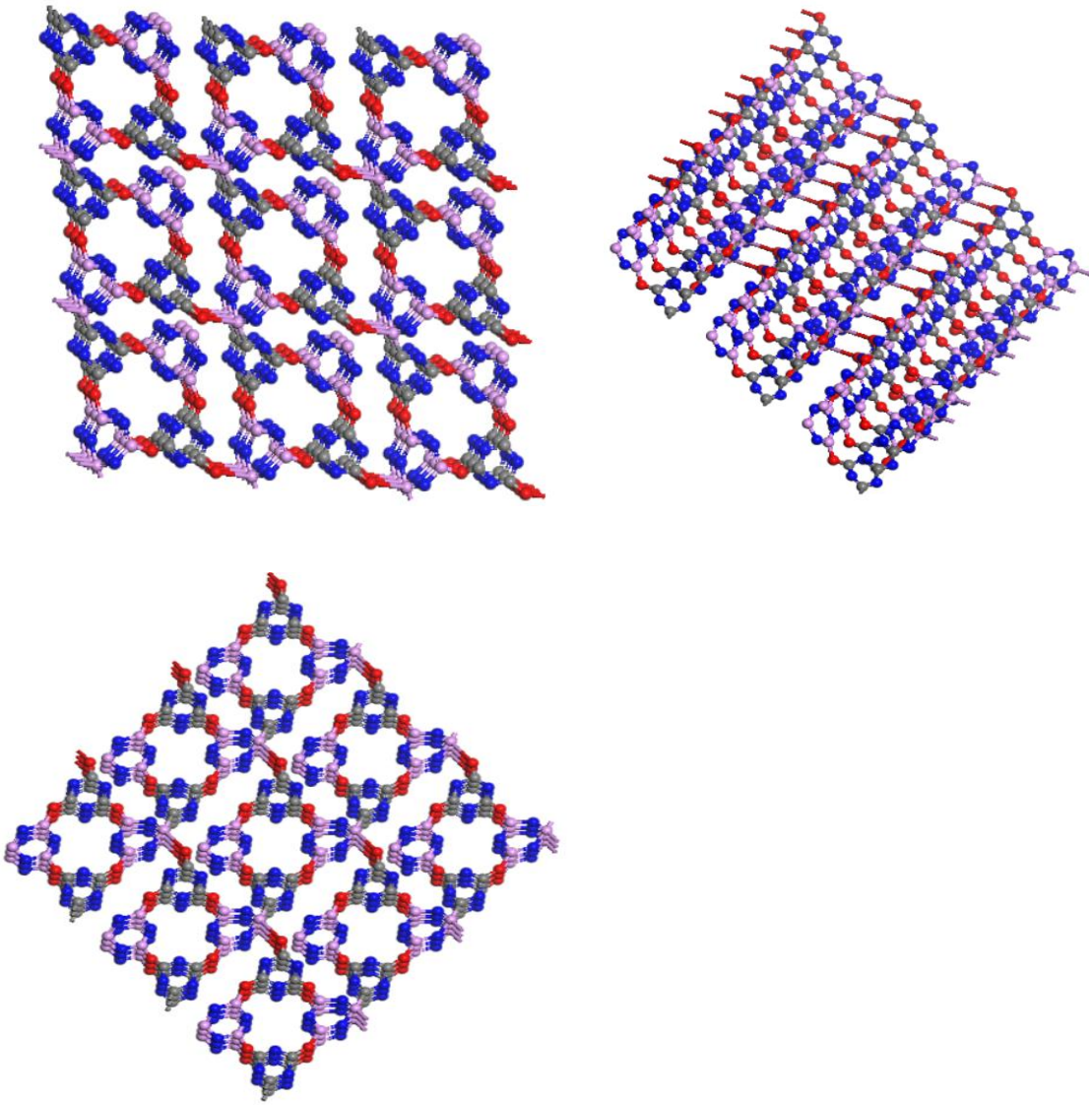

Fig. S12. Chemical skeleton of D1M4-PC sample (N element (Blue), P element (Pink), C element (Gray), and O element (Red)).

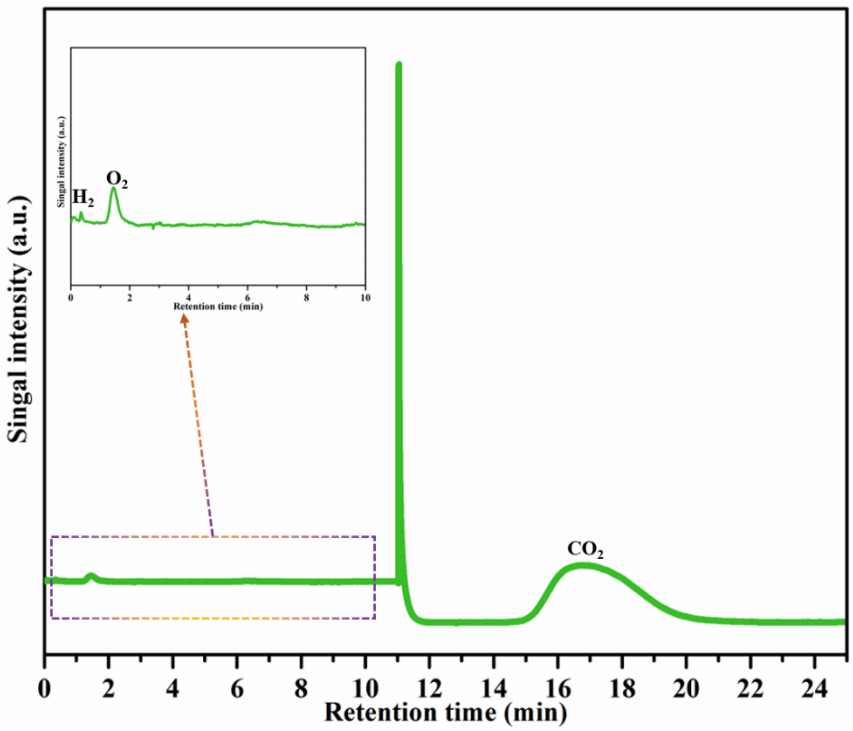

Fig. S13. GC spectrum of D1M4-PC sample with a thermal conductivity detector (TCD).

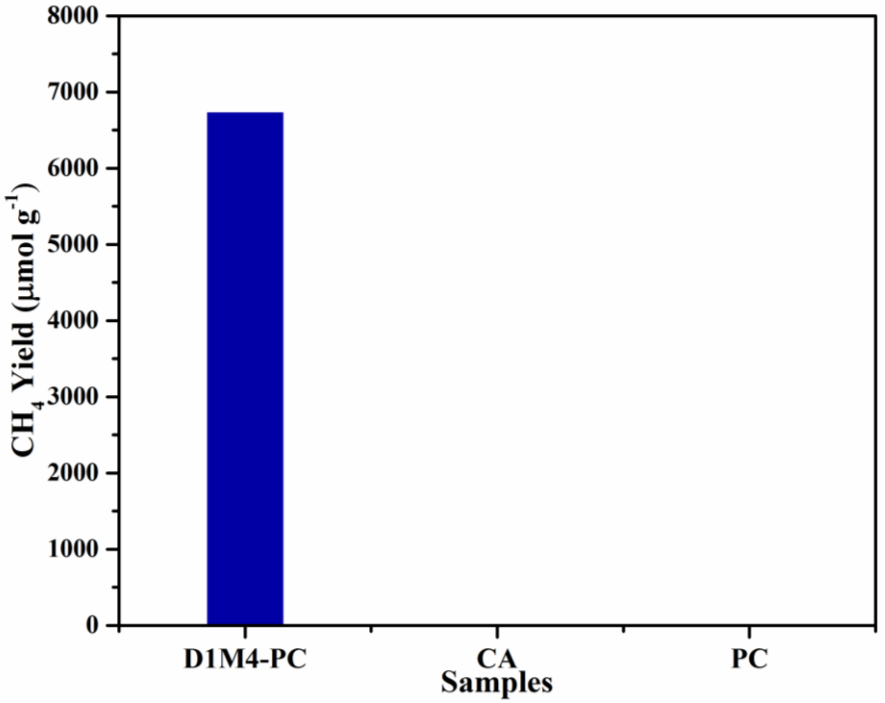

Fig. S14. Photocatalytic CO_2 conversion rates for cyanuric acid (CA), hexachlorocyclotriphosphazene (PC), and D1M4-PC samples.

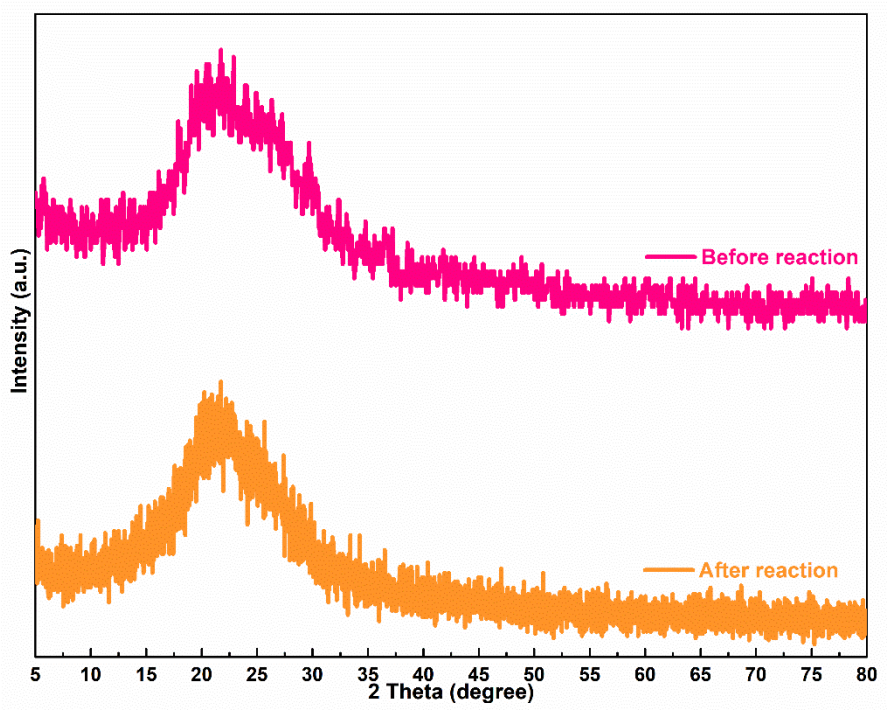

Fig. S15. XRD patterns of D1M4-PC sample before and after the stability test.

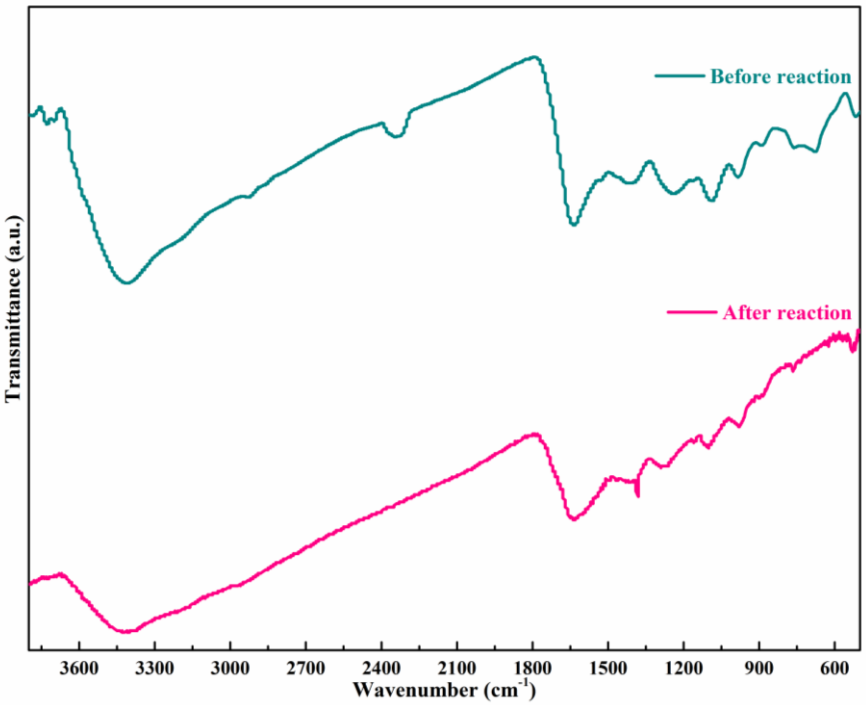

Fig. S16. FT-IR spectra of D1M4-PC sample before and after the stability test.

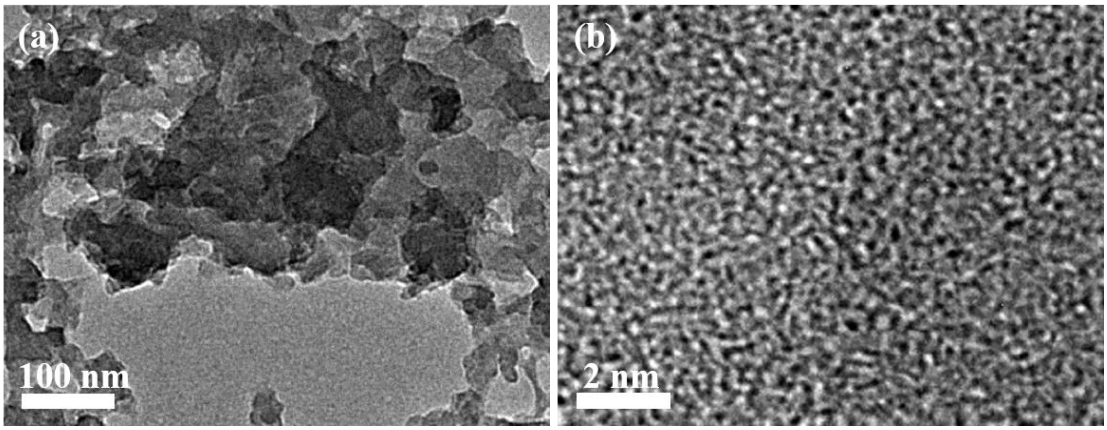

Fig. S17. TEM (a) and HRTEM (b) of D1M4-PC sample after the stability test.

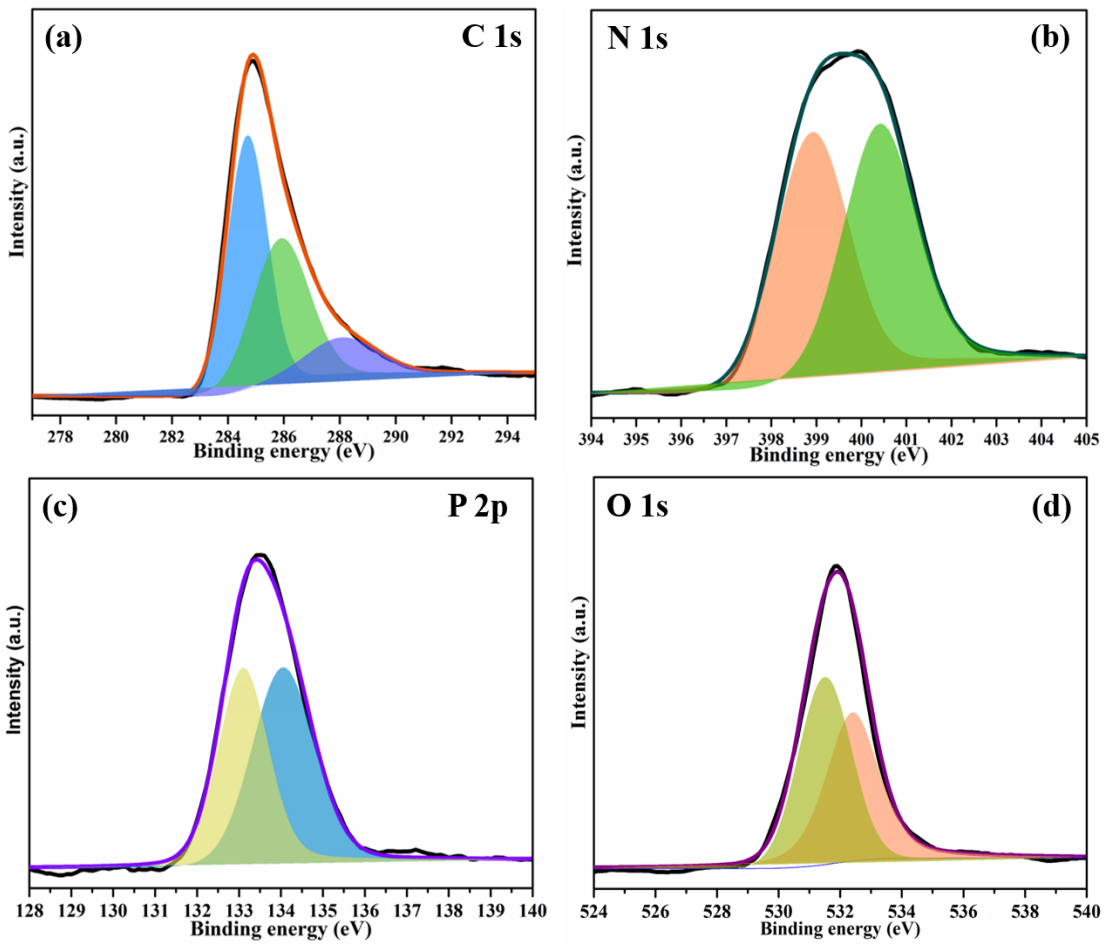

Fig. S18. XPS spectra of D1M4-PC after the stability test: (a) C 1s, (b) N 1s, (c) P 2p and (d) O 1s.

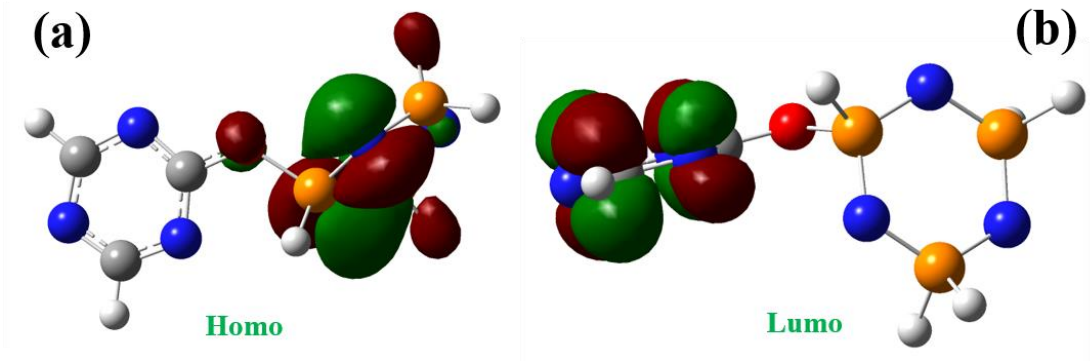

Fig. S19. Frontier molecular orbital picture of D-A structure (a: Homo, b: Lumo) from DFT calculation using the 6-31(d,p) basis set in the B3LYP method.

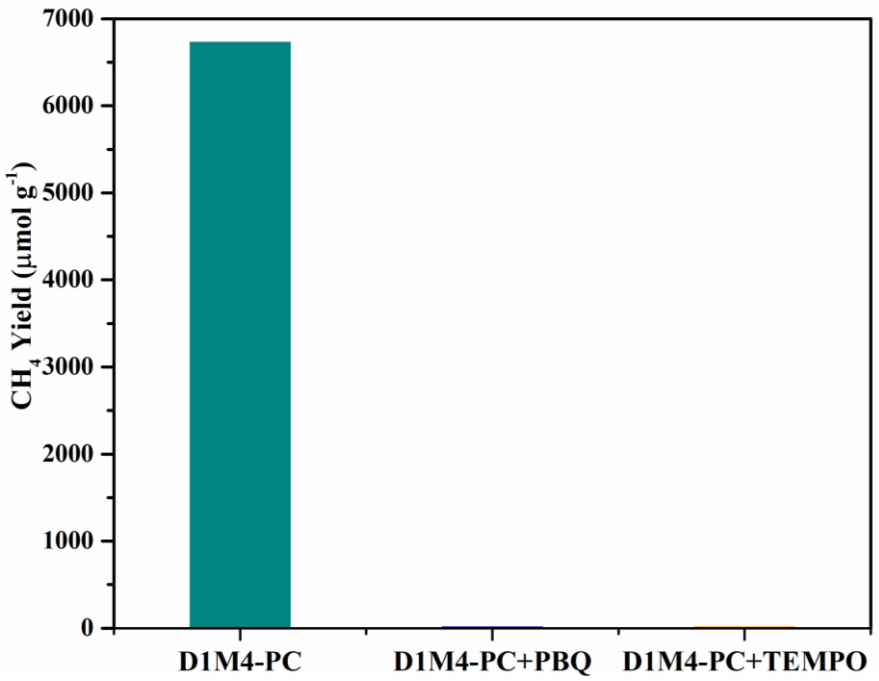

Fig. S20. Free radical trapping experiment of D1M4-PC.

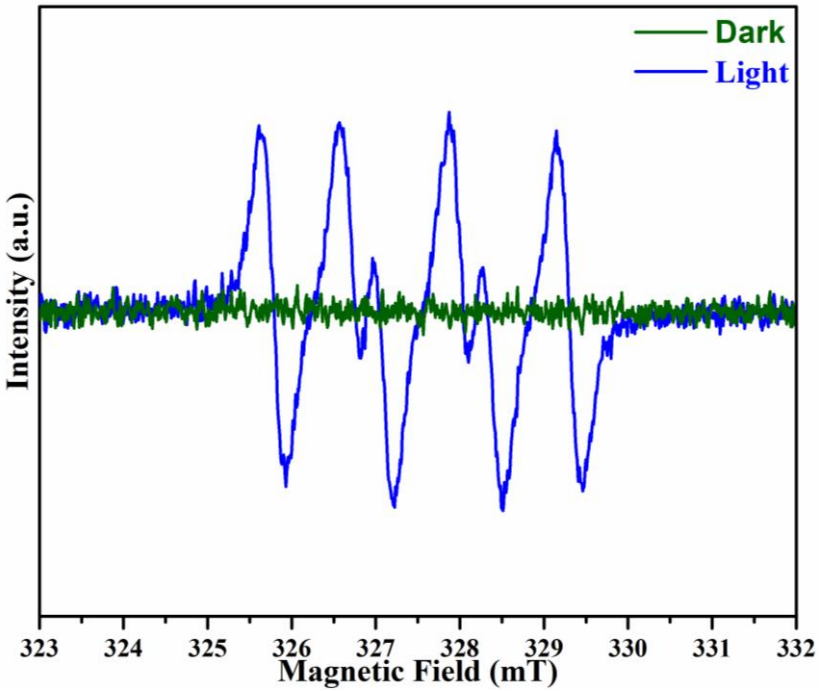

Fig. S21. ESR spectra of $\cdot O_2^-$ in D1M4-PC sample.

Computational Details

All computations were performed under the framework of Density Functional Theory (DFT)using the Gaussian 16 or MS software package of programs. In our calculation, the simplest possible repetitive unit consisting of single cyanuric acid and single phosphonitrile was taken into consideration. Molecular geometries were optimized using B3LYP(g) and energy was calculated using B3LYP(g,d).

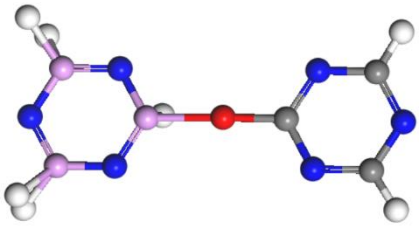

Ball-stick representation of D1M4-PC using in DFT calculate.

DFT-optimized geometry of D1M4-PC (singlet).

Atom	x	y	z
N	**-1.73872062**	**-1.35046377**	**0.75296857**
P	**-0.53993591**	**-0.29972954**	**0.85831432**
N	**-0.80039354**	**1.22382279**	**0.44771370**
P	**-2.09534569**	**1.61247668**	**-0.44775712**
N	**-3.19608839**	**0.47345742**	**-0.74794073**
P	**-3.01949620**	**-1.02870329**	**-0.18640248**
O	**0.67292633**	**-0.94381765**	**-0.12431486**
N	**2.71010837**	**-0.89158193**	**-1.11169532**
C	**3.94855208**	**-0.40013600**	**-1.06668428**
N	**4.43803826**	**0.44484605**	**-0.14979670**
C	**3.55297435**	**0.78465926**	**0.79110675**
N	**2.28907925**	**0.36454747**	**0.86756258**
C	**1.92718401**	**-0.46572955**	**-0.11712745**
H	**3.88865280**	**1.46576892**	**1.57010289**
H	**4.62653473**	**-0.71707730**	**-1.85642504**
H	**-3.05934679**	**-1.93172640**	**-1.27109059**
H	**-4.17133737**	**-1.41013015**	**0.52995761**
H	**0.04548405**	**-0.37993801**	**2.11765638**
H	**-2.71249428**	**2.72633137**	**0.15749498**
H	**-1.66566256**	**2.17149670**	**-1.67095298**

Part of the Gaussian output file:
Mulliken charges:

1	N	-0.654682
2	P	0.950038
3	N	-0.659825
4	P	0.782871
5	N	-0.679479
6	P	0.791086
7	O	-0.535625
8	N	-0.410488
9	C	0.246219
10	N	-0.396266
11	C	0.254717
12	N	-0.434669
13	C	0.668566
14	H	0.131480
15	H	0.131683
16	H	-0.040569
17	H	-0.038070
18	H	-0.025847
19	H	-0.038606
20	H	-0.042534

Sum of Mulliken charges = 0.00000

Mulliken charges with hydrogens summed into heavy atoms:

		1
1	N	-0.654682
2	P	0.924191
3	N	-0.659825
4	P	0.701731
5	N	-0.679479
6	P	0.712448
7	O	-0.535625
8	N	-0.410488
9	C	0.377902
10	N	-0.396266
11	C	0.386197
12	N	-0.434669
13	C	0.668566

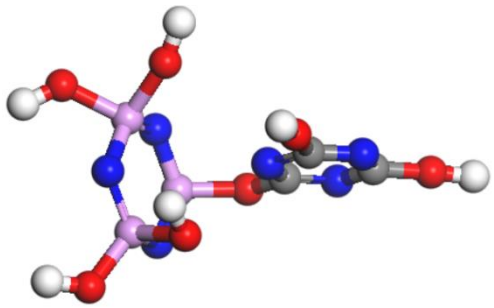

Ball-stick representation of D1M4-PC using in DMol3 calculate for electrostatic potential energy.

DMol3-optimized geometry of D1M4-PC.

Atom	x	y	z
N	**9.33811063316486**	**9.66674496293331**	**4.10215850701181**
P	**11.86123407225155**	**11.01813324913500**	**3.13212458543765**
N	**14.55799073122141**	**10.18170191391016**	**4.21148691688898**
P	**14.65973190960400**	**8.61945797156388**	**6.85217485181998**
N	**12.12751877258279**	**7.26771451133700**	**7.87799970391317**
P	**9.42592311460137**	**8.09195476979524**	**6.73483436788998**
O	**11.53178927674260**	**14.21711780563321**	**3.26022167581976**
N	**11.09485685168512**	**17.95297030013372**	**5.30647346047805**
C	**10.94540236765615**	**19.11600686792085**	**7.54152827550298**
N	**11.05467915210532**	**18.02516738689458**	**9.83236970869192**
C	**11.33538492508340**	**15.51485145134674**	**9.73637604917056**
N	**11.50545008692956**	**14.10654207824779**	**7.64032909105767**
C	**11.37509643300762**	**15.44243437589849**	**5.48058228852209**
O	**11.38407282485340**	**14.18509407208206**	**12.26061050926874**
O	**10.66491312138720**	**21.95445937937583**	**7.45847445704100**
H	**10.55303384580295**	**24.04852894507905**	**7.50606401775154**
H	**11.58878701282122**	**13.09603680121291**	**14.04160896076139**
O	**17.59844719488438**	**6.89047848543519**	**7.53392253036154**
O	**8.66765664013738**	**4.76544252952172**	**7.40531609075861**
H	**17.81729403982867**	**4.84455882392281**	**7.94163308099888**
H	**9.76479786457199**	**2.98767494656442**	**7.59434712792057**
H	**11.26528696688916**	**11.46273397493783**	**0.45557989096986**
O	**14.56535851826974**	**10.90717646981483**	**9.46897351914460**
O	**6.82141220810108**	**9.45610551224441**	**8.59112453865332**
H	**4.99720291053773**	**9.95338570237613**	**9.49935465172530**
H	**13.45008646014807**	**9.84976319014228**	**10.89654303571155**

Table S1. The comparation of photocatalytic CO_2 reduction activity among some representative photocatalysts reported in the literatures over recent years and ***this work***.

Photocatalyst	Light source	Major Product (Yield and Rate)	CH_4 selectivity	Ref.
D1M4-PC	**300 W Xenon lamp ($\lambda \geq 420$ nm)**	**CH_4 (6733 μmol g^{-1})**	**>99%**	**This work**
Cu_2O-111-Cu^0	300 W Xenon lamp ($\lambda \geq 420$ nm)	CH_4 (150 μmol g^{-1})	97%	[1]
CuPP	white LED ($\lambda > 400$ nm)	CO (16.1 μmol g^{-1})	95%	[2]
V_S-$CuInS_8$	Visible light	CH_4 (209 μmol g^{-1})	100%	[3]
MOF-525-Co	300 W Xenon lamp (400 nm < λ <800 nm	CO (1210 μmol g^{-1})	40.9%	[4]
Cu_2O@Cu@UiO-66-NH_2	300 W Xenon lamp (λ >400 nm)	CO (104.5 μmol g^{-1})	61.4%	[5]
5%APCN/CdSe−DETA	300 W Xenon lamp (λ >420 nm)	CH_4 (25.9 μmol g^{-1})	25.3%	[6]
CMP-BT^3	300 W Xenon lamp (λ >420 nm)	CO (50 μmol g^{-1})	81.6%	[7]
MIL-101(Cr)−Ag	300 W Xe lamp (400 nm < λ < 780 nm)	CH_4 (427.5 μmol g^{-1})	62.9%	[8]
rGO-coated Ag/Cu_2O	300 W Xe lamp (λ>380 nm)	CH_4 (82.6 μmol g^{-1})	90%	[9]
$Cs_2AgBiBr_6$/$Ti_3C_2T_x$	300 W Xe lamp ($\lambda > 420$ nm)	CO (50.6 μmol g^{-1})	68%	[10]

[1] Y. Deng, C. Wan, C. Li, Y. Y. Wang, X. Y. Mu, W. Liu, Y. P. Huang, P. K. Wong, and L. Q. Ye, Synergy effect between facet and zero-valent copper for selectivity photocatalytic methane formation from CO_2, ACS Catal. 12 (2022) 4526-4533.
[2] H. Yuan, B. Cheng, J. Lei, L. Jiang, Z. Han, Promoting photocatalytic CO_2 reduction with a molecular copper purpurin chromophore, Nat. Commun. 12 (2021) 1835-1844.

[3] X. D. Li, Y. F. Sun, J. Q. Xu, Y. J. Shao, J. Wu, X. L. Xu, Y. Pan, H. X. Ju, J. F. Zhu and Y. Xie, Selective visible-light-driven photocatalytic CO_2 reduction to CH_4 mediated by atomically thin $CuIn_5S_8$ layers, Nat. Energy. 4 (2019) 690-699.
[4] H. B. Zhang, J. Wei, J. C. Dong, G. G. Liu, L. Shi, P. F. An, G. X. Zhao, J. T. Kong, X. J. Wang, X. G. Meng, J. Zhang, J. H. Ye, Efficient visible-light-driven carbon dioxide reduction by a single-atom implanted metal-organic framework, Angew. Chem., Int. Ed. 55 (2016) 14310-14314.
[5] S. Q. Wang, X. Y. Zhang, X. Y. Dao, X. M. Cheng, W. Y. Sun, Cu_2O@Cu@UiO-66-NH_2 ternary nanocubes for photocatalytic CO_2 reduction, ACS Appl. Nano Mater. 3 (2020) 10437-10445.
[6] Y. Huo, J. F. Zhang, K. Dai, C. H. Liang, Amine-modified S-Scheme porous g-C_3N_4/CdSe–diethylenetriamine composite with enhanced photocatalytic CO_2 reduction activity, ACS Appl. Energy Mater. 4 (2021) 956-968.
[7] C. Yang, W. Huang, L. C. Silva, K. Zhang, X. C. Wang, Functional conjugated polymers for CO_2 reduction using visible light, Chem. Eur. J. 24 (2018) 17454-17458.
[8] F. Guo, S. Z. Yang, Y. Liu, P. Wang, J. Huang, W. Y. Sun, Size engineering of metal-organic framework MIL-101(Cr)-Ag hybrids for photocatalytic CO_2 reduction, ACS Catal. 9 (2019) 8464-8470.
[9] Z. L. Tang, W. J. He, Y. L. Wang, Y. C. Wei, X. L. Yu, J. Xiong, X. Wang, X. Zhang, Z. Zhao, J. Liu, Ternary heterojunction in rGO-coated Ag/Cu_2O catalysts for boosting selective photocatalytic CO_2 reduction into CH_4, Appl. Catal. B Environ. 311 (2022) 121371-121385.
[10] Z. P. Zhang, B. Z. Wang, H. B. Zhao, J. F. Liao, Z. C. Zhou, T. H. Liu, B. C. He, Q. Wei, S. Chen, H. Y. Chen, D. B. Kuang, Y. Li, G. C. Xing, Self-assembled lead-free double perovskite-MXene heterostructure with efficient charge separation for photocatalytic CO_2 reduction, Appl. Catal. B Environ. 312 (2022) 121358-121367.